ORNL/TM-8233

ornl

OAK RIDGE NATIONAL LABORATORY

UNION CARBIDE

Theoretical Characterization of a Dual-Purpose Gamma Thermometer for Local Power-Generation Measurement in an LMFBR

J. O. Johnson
T. J. Burns

OPERATED BY
UNION CARBIDE CORPORATION
FOR THE UNITED STATES
DEPARTMENT OF ENERGY

DISCLAIMER

Printed in the United States of America. Available from
National Technical Information Service
U.S. Department of Commerce
5285 Port Royal Road, Springfield, Virginia 22161
NTIS price codes—Printed Copy: A04; Microfiche A01

ORNL/TM-8233
Distribution Category UC-79d

Contract No. W-7405-eng-26

Engineering Physics Division

ORNL/TM--8233

DE82 013371

THEORETICAL CHARACTERIZATION OF A DUAL-PURPOSE GAMMA THERMOMETER FOR LOCAL POWER-GENERATION MEASUREMENT IN AN LMFBR

J. O. Johnson*
T. J. Burns

Date Published - April 1982

NOTICE This document contains information of a preliminary nature. It is subject to revision or correction and therefore does not represent a final report.

*University of Tennessee
Department of Nuclear Engineering
Knoxville, TN 37916

Research Sponsored by
U.S. Department of Energy
under Contract No. W-7405-eng-26
with the Union Carbide Corporation

OAK RIDGE NATIONAL LABORATORY
Oak Ridge, Tennessee 37830
operated by
UNION CARBIDE CORPORATION
for the
DEPARTMENT OF ENERGY

THIS PAGE

WAS INTENTIONALLY

LEFT BLANK

TABLE OF CONTENTS

THIS PAGE

WAS INTENTIONALLY

LEFT BLANK

ABSTRACT

A preliminary analytical and computational study was performed to investigate the potential of a modified gamma thermometer (GT) as both a local power level monitor and a sodium flow blockage monitor for a Liquid Metal Fast Breeder Reactor. This study consisted of two fundamental parts: a radiation field characterization and a thermal-hydraulic analysis.

The radiation transport analysis was performed to determine the volumetric heat source within the GT resulting from gamma and neutron heating. Both fission-product decay gammas and neutron-induced gammas were treated in the analysis, as well as the direct neutron heating effect.

Further, a sensitivity analysis was performed to characterize the origin of the neutron-induced gammas (by material) contributing to the volumetric heat source. This source was then utilized to perform a series of thermal-hydraulic calculations to model certain reactor transients of interest (i.e., reactor scram and sodium flow blockage) in order to characterize the gamma thermometer response relative to local power level monitoring and sodium flow blockage indication.

The results of this preliminary study confirm the feasibility of utilizing the GT as an in-core local power level measurement device. However, the proposed signal for monitoring sodium flow blockage was shown to be insignificant and therefore uninterpretable. As a local power level monitor, however, the results provide encouragement and incentive to pursue the GT as a viable nuclear instrument.

I. INTRODUCTION

1.0 Background

The requirement for determining the local power generation rate within a nuclear reactor core is typically mandated by various material limitations of the reactor's fuel assemblies (i.e., cladding burnout, critical heat flow, etc.). For Light Water Reactors (LWRs) this requirement has been met through the use of in-core instrumentation such as Self-Powered Neutron Detectors (SPNDs) and/or fission chambers. Recently, however, there has been an increased interest in the use of an alternate instrument, the gamma thermometer (GT), for the measurement of the local power generation rate in LWRs.[1,2] The GT, originally developed for heavy water reactors, has been proposed as a replacement for the SPNDs currently utilized in LWRs. Since the current design philosophy of Liquid Metal Fast Breeder Reactors (LMFBRs) mitigates against use of any in-core instrumentation, a brief feasibility study of the GT in an LMFBR was undertaken to provide data for possible future LMFBR designs.

The increased interest in the GT for LWR applications is related to the spatial variations of the thermal-neutron and gamma fluxes within a fuel assembly. The thermal-neutron flux exhibits a large amount of structure as a function of position within the fuel assembly, whereas the gamma flux shows very little structure. The use of a local power level indicator based on less-structured gamma flux (produced via neutron interaction and the decay of fission products) has the potential for improving the accuracy of the measurement and thereby reducing the uncertainty regarding the power level. It is therefore postulated that a reduction of 5-7% in the uncertainty may be possible using the gamma thermometer in an LWR.

Clearly, the neutron flux exhibits much less structure in an LMFBR than does the thermal flux in an LWR. Hence the use of the GT would offer less potential reduction in uncertainty in fast reactors. The proposed GT does, however, possess an important advantage over SPNDs and fission chambers for LMFBRs: it contains no depletable materials (such as those used in the aforementioned sensors), and therefore has the potential for a longer operating life in an LMFBR core environment without appreciably

sacrificing reliability of signal interpretation. Furthermore, through increased reliability and longer life, the GT offers the possibility of limiting to the current levels occupational exposure resulting from instrument maintenance or replacement during scheduled fuel reloading.

Another incentive for investigating the potential of a GT-based sensor for local power generation monitoring in an LMFBR is the recent recognition that, for PWRs in particular, the GT has the potential of serving as a dual-purpose instrument.[3,4] In this context, a modified version of the GT appears to have the capability of measuring both the local heat generation rate (LHGR) and the adequacy of the core cooling mechanism via the coolant heat transfer coefficient. Thus, one of the possible LMFBR uses of the GT considered in this study was that of a sodium flow blockage detector — a situation analogous to the reduction of heat transfer capacity considered for the PWR.

The most significant disadvantage regarding the use of the GT in an LMFBR is the accessibility of the generated signal. This disadvantage however is not unique to the GT, but would be inherent in any in-core instrumentation. Current LMFBR design philosophy (as well as the physical configuration of current or proposed LMFBRs) preclude the use of instrumentation which is inserted into the core. Moreover, the desire to minimize the number of penetrations in the reactor vessel to the extent possible inhibits the use of the typical PWR option - insertion from below the core. Although certain means of overcoming these limitations can be envisioned (i.e., incorporation of the GT leads as part of a control rod drive assembly or use of remote signal transmission technology), a detailed discussion of the practical engineering problems inherent in the use of the GT in LMFBRs is beyond the scope of this study. The work reported below is directed at establishing the feasibility of the GT (i.e., the presence of a signal and its interpretability) in a generic LMFBR environment.

1.1 Technical Summary of the Proposed Gamma Thermometer

1.1.1 Physical Description

The GT consists of a hollow, cylindrical, stainless steel rod of a length equal to or greater than the height of the reactor core. At

intervals along the rod, annuli of material are removed by machining. A series of differential thermocouples (TCs) are then located at each annulus location, with the TCs and associated electrical leads positioned in the hollow center of the rod. Magnesium oxide (MgO) is utilized as a packing and insulating material in the central cavity. After it is assembled, zircalloy cladding is swaged onto the exterior in an inert atmosphere (typically argon). The resulting device (Fig. 1) then would be inserted into a fuel assembly, usually in a central rod position.

1.1.2 Use of the Gamma Thermometer as a Local Power Level Monitor (PLM)

During operation of a nuclear reactor, the various neutron interaction processes (i.e., fission, capture, etc.), together with fission-product decay, produce gamma radiation. The placement of the GT within a fuel assembly would allow some fraction of these gamma rays to interact with the stainless steel body of the proposed GT, depositing energy and thereby producing heat. The resulting heat is then transferred from the device to the coolant in which it is immersed. The presence of this volumetric heat source, coupled with the illustrated design, will produce a temperature distribution within the device itself. The incorporated thermocouples are used to measure the magnitude of this temperature distribution at two locations (T_{Hot} and T_{Cold} in Fig. 1) within the standard GT, with the difference between T_{Hot} and T_{Cold} being related to the localized heat generation rate ΔV_1. The relation between the localized heat generation rate and the measured temperature difference can be roughly approximated as:

$$\Delta T = qL^2/2k$$

where

ΔT = temperature differential between thermocouple junctions, °C,

q = heat generation within the thermometer, W/cm^3,

L = distance between thermocouple junctions, in cm,

k = thermal conductivity, in W/cm °C.

Since q is induced (in part) by the production of gamma rays in fission and fission-product decay (both of which contribute to the linear power of the fuel), Eq. (1) indicates that the temperature difference in the GT can be related to the local heat generation rate.

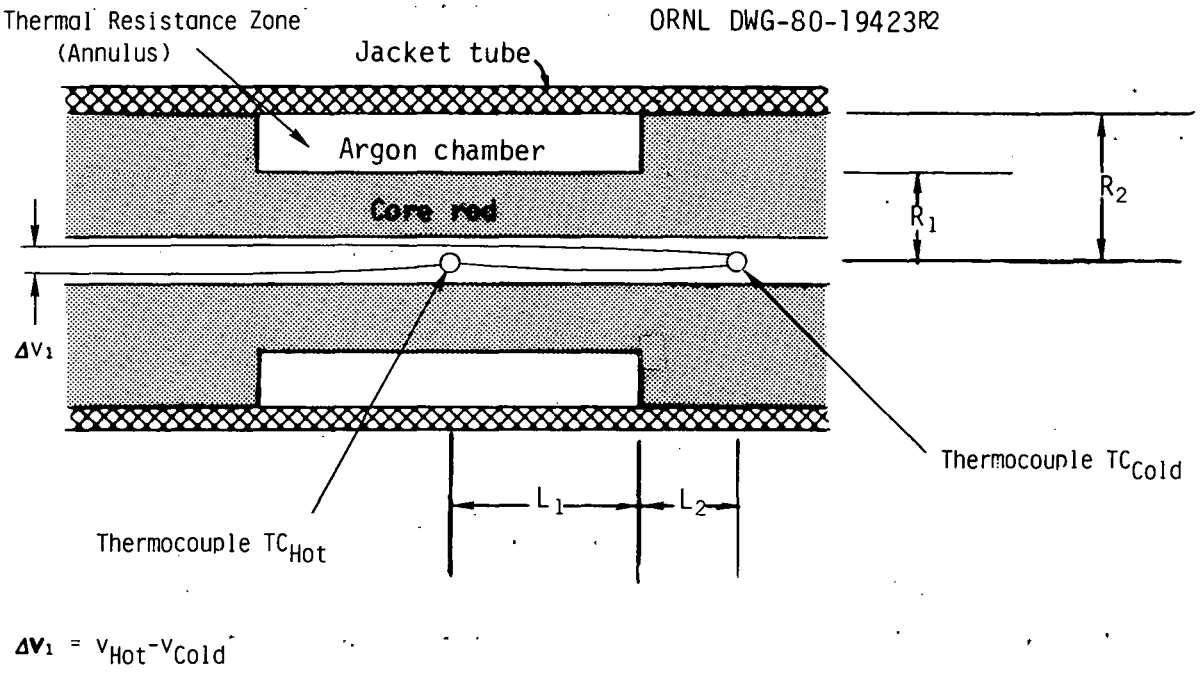

Fig. 1. Schematic of the Standard Gamma Thermometer.

1.2 Objectives and Scope of Investigation

While the use of the GT as a local power monitoring device in an LMFBR is intuitively appealing, it must be noted that the basic arguments advanced in the above discussion are qualitative and not quantitative. Further investigation, both analytical and computational, is clearly required to establish its feasibility for this application.

This initial investigation, aimed at a quantitative characterization of the GT, included a simplified one-dimensional analytical calculation relating the temperature difference to the various properties (e.g. thermal power, etc.) of the system. Further, a series of two-dimensional transport calculations was executed to relate the volumetric heat source within the GT to the reactor power, and a series of thermal hydraulic calculations utilizing the volumetric heat source was executed to characterize the GT temperature response. This latter series of calculations was aimed primarily at establishing the degree to which the proposed local power level signal was independent of the thermal-hydraulic properties of the coolant. The primary objective of this initial analysis was to

establish the relationship between the GT signal and the local power generation rate — a necessary prerequisite to licensing the GT for routine use. A secondary objective of the computational analysis was to investigate the potential of a modified version of the GT for detecting changes in the fluid characteristics, which could indicate a flow blockage within the nuclear core. The computational effort aimed at realizing these objectives proceeded along two parallel paths, the first dealing with the characterization of the radiation transport from the fuel pins to the detector and the subsequent heat deposition, and the second concerning the thermal-hydraulic behavior of the GT itself.

It should be noted, however, that the level of analysis required to license the gamma thermometer is beyond the scope of this report. Rather, the goal of this study was to establish the underlying feasibility of the GT as an indicator of the LHGR within the core through detailed calculational work and to investigate its potential as a flow blockage indicator so that the pursuit of further efforts for either application could be justified.

II. THEORETICAL ANALYSIS OF THE GAMMA THERMOMETER

The usefulness of the GT as an indicator of local power generation is dependent on the ability of the device to reliably measure the LHGR for a variety of thermal-hydraulic conditions. Consequently, the characteristic response used for the power level indicator should be a strong function of the reactor power and a weak function of other parameters such as the heat transfer characteristics and hydraulic environment of the GT.

A one-dimensional steady-state analytical calculation was performed on the proposed gamma thermometer design (see Fig. 1) to characterize the thermocouple signals. (The detailed description of the calculation is appended to this report.) The results of the analysis, shown below in Eqs. (2) and (3), depict the temperature at both TC locations as functions of power and heat transfer characteristics:

$$(T_{Hot} - T_{Coolant}) = \frac{qL_1^2}{2k} + \frac{\frac{qL_1R_1^2}{kmR_2^2}\,(1 + e^{-2mL_2})}{(1 - e^{-2mL_2})} + \frac{q}{m^2k} \qquad (2)$$

$$(T_{Cold} - T_{Coolant}) = \frac{\frac{2qL_1R_1^2}{kmR_2^2}e^{-mL_2}}{(1 - e^{-2mL_2})} + \frac{q}{m^2k} \quad , \qquad (3)$$

where $m^2 = \frac{hP}{kA}$ and the remaining terms are defined in Fig. 1 or in the Appendix. As stated above, the difference between the two TC readings is utilized to infer the local heat generation rate. Subtracting Eq. (3) from Eq. (2) yields:

$$(T_{Hot} - T_{Cold}) = \frac{qL_1^2}{2k} + \frac{\frac{qL_1R_1^2}{kmR_2^2}(1 + e^{-2mL_2}) - 2e^{-mL_2}}{(1 - e^{-2mL_2})} \quad , \qquad (4)$$

which, as desired, is a strong function of the local power (via q) and a weak function of the heat transfer properties (via m). The functional dependence of the GT signal on local power and its relative insensitivity to the heat transfer properties is depicted graphically in Fig. 2. As indicated, a relatively large change in the heat transfer coefficient (±20% represented by the dotted lines in Fig. 2) results in a very small change in the relationship between signal and power generation rate.

Equation (4) and Fig. 2 indicate that theoretically the GT can function as a local power level monitoring device. The use of Eq. (4) as a response provides an indication of the local heat generation rate in the reactor region in the vicinity of the GT. Hence, by using "strings" of active locations spaced radially within the reactor core, a power map can be obtained with the GT.

Although the above theoretical analysis illustrates the feasibility of utilizing the GT as a power level measuring device, many of the simplifying assumptions used in the analysis must be evaluated as to their effect on the results. Due to the coupled nonlinear inhomogeneous nature of the GT heat conduction problem, the multi-dimensional analysis was treated via numerical techniques. In particular, a radiation transport analysis was used to characterize the volumetric heat generation rate as a function of reactor power, and a thermal-hydraulic analysis was used to relate the exterior heat transfer coefficient to changes in the coolant flow.

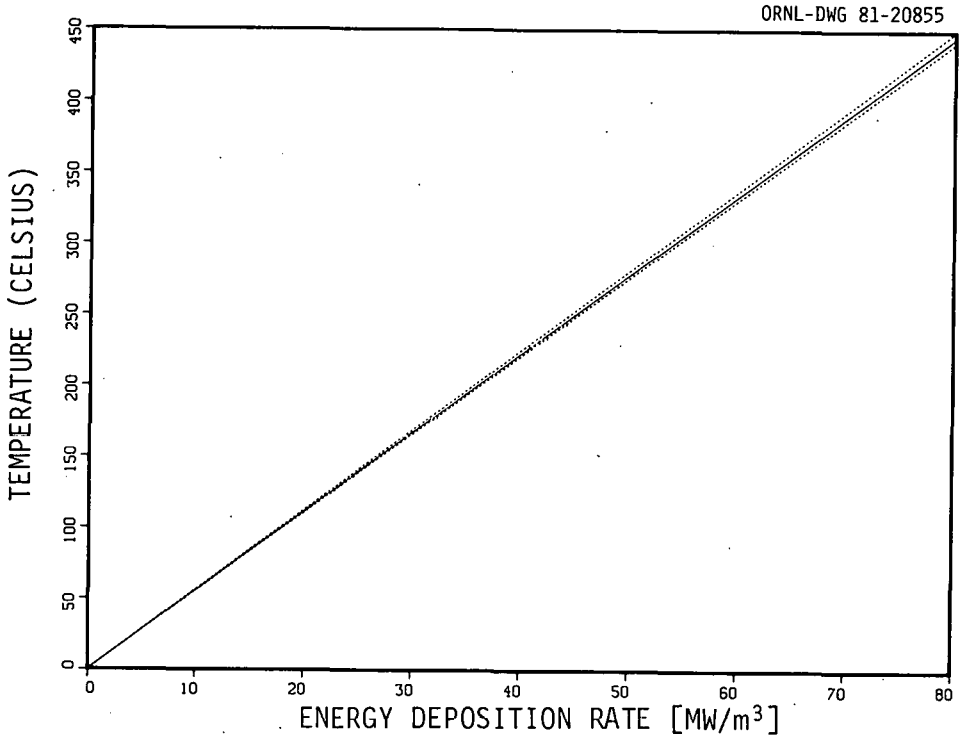

Fig. 2. Theoretical Power Level Monitor Response Characteristics of the Gamma Thermometer.

III. RADIATION TRANSPORT ANALYSIS

As noted previously, a primary objective of this study is to relate the energy deposition within the GT [q in Eqs. (1-4)] to the local heat generation rate occurring within the fuel pins. Such a characterization must include the origin of the particles involved (i.e., geometrically within the reactor), the source of the particles (i.e., neutron-induced reactions or fission-product decay), and also the manner in which the particles (which can be viewed as containing information regarding the state of the reactor) actually reach the detector. The results of just such a characterization are reported in this section.

A prototypic LMFBR fuel assembly consisting of 217 pins in a hexagonal lattice was selected as the basis for this investigation. The design parameters for this assembly are given in Table 1. The central pin of the hexagonal array was replaced with the GT; the remaining pins contained plutonium-uranium dioxide fuel. The two-dimensional R-Θ model shown in Fig. 3 was used in the analysis to represent the axial midplane of the hexagonal pin array shown in Fig. 4. Because a symmetric configuration

Table 1. Design Parameters Used in the Radiation Transport and Thermal-Hydraulic Calculations

Rated heat output (core), MW(th)	975
System pressure (nominal), Pa	1.0342×10^5
Average coolant flow velocity, m/s	7
Coolant inlet temperature, °C	388
Coolant outlet temperature, °C	535
Fuel assembly pitch, mm	120.9
Overall dimensions of fuel assembly (external flat to flat), mm	116.2
Overall dimensions of fuel assembly (internal flat to flat), mm	110.1
Number of fuel rods per assembly	216*
Active fuel length (core), mm	914.4
Fuel rod pitch, mm	7.31
Outside diameter of fuel rod, mm	5.84
Cladding thickness (SS-316), mm	0.38
Fuel pellet diameter, mm	4.92
Diametrical gap (between fuel pellet and clad), mm	0.17
Fuel rod radial spacing, mm (wires wrapped around fuel pins in helical fashion)	1.42
Clearance between fuel rods, mm	1.47
Clearance between fuel rods at wires, mm	0.04
Fuel pellet (plutonium-uranium dioxide) density, % of theoretical	91.3
Average fuel discharge burnup, MWd/kg	110.2

*Assumes that one fuel rod is replaced with the gamma thermometer.

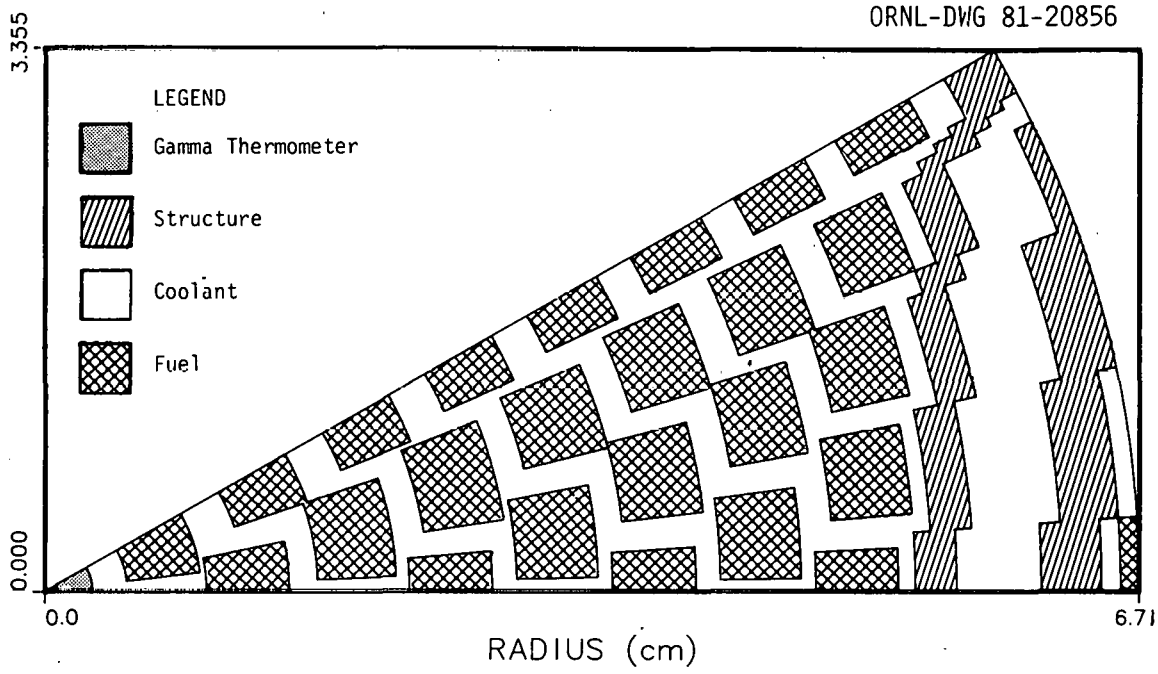

Fig. 3. Computational Model of the Prototypic LMFBR Fuel Assembly Used for the Radiation Transport Analysis.

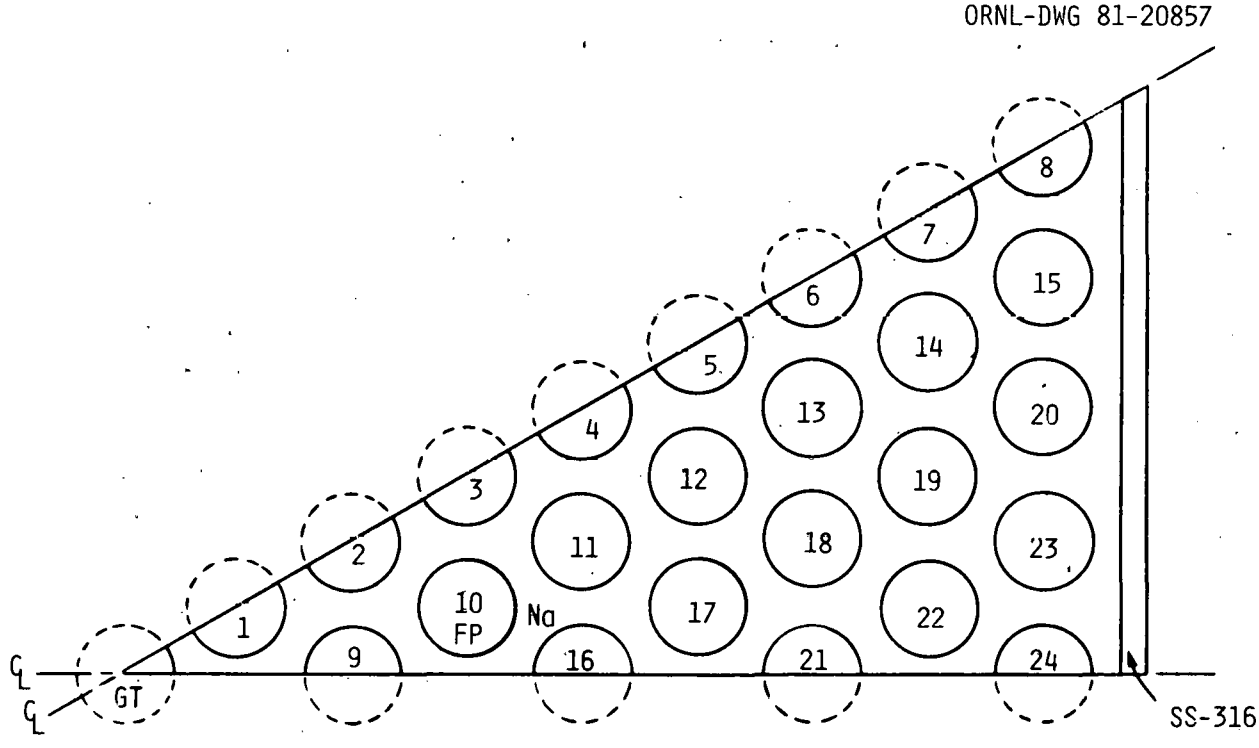

Fig. 4. Actual Hexagonal Model of the Prototypic LMFBR Fuel Assembly with Gamma Thermometer in the Central Rod Position and Fuel Pins Numbered 1-24 (one-twelfth Symmetry, Excluding Dashed Lines).

was assumed, only one-twelfth of the assembly was actually calculated. The materials and number densities comprising the various regions are given in Table 2. In the numerical transport analysis, a 2 x 10 array of nodes was used within the GT itself for the purpose of obtaining the spatial distribution of the energy deposition.

The difference between the transport processes of neutrons and gamma radiation in sodium limits the usefulness of standard reactor core analysis methods (i.e., diffusion theory) to accurately model the transport of gamma rays. However, the methods typically employed in radiation shielding applications (e.g. particle transport theory) are appropriate calculational tools.

Nuclear parameters for the various materials were taken from the 51-neutron-energy-group, 25-gamma-group coupled cross-section library.[5] This library has been used extensively for LMFBR shielding calculations. The AMPX-II[6] modular cross-section processing system was utilized to reduce the 51n-25γ group library to a 9n-25γ group library with one thermal group (and hence no upscatter).

In order to calculate the energy deposition rate within the stainless steel core of the GT, two sources of gamma radiation must be considered: the gammas resulting from neutron-induced reactions (fission, capture, and inelastic scattering) and the gammas produced by the decay of the various fission products. The contributions from these two sources were calculated separately. The response function utilized for both sources of gamma radiation was the energy deposition rate for stainless steel (SS-316) given in Table 3. The energy deposition rate resulting from the neutron-induced reactions was computed via an eigenvalue calculation using the coupled neutron-gamma library and normalized to a fission rate corresponding to 262.47 W/cm. All radiation transport calculations were performed using the DOT-IV[7] computer code. In all cases, a P_3 scattering approximation and an S_8 quadrature set (48 directions) were employed.

The fission-product decay contribution was calculated using only the gamma groups and assuming a uniform fixed source in each fuel pin. The gamma energy spectrum and source strength for the fission-product contribution were determined using ORIGEN[8] at a burnup of approximately

Table 2. Materials and Number Densities Used in Radiation Transport Calculations

Mixture	Material	Number Density (atoms/cm^3)
Sodium Coolant	Na	2.3055 + 22*
SS-316	C	1.1733 + 20
	Mn	1.7179 + 21
	Si	1.6800 + 22
	Cr	1.5428 + 22
	Ni	1.1253 + 22
	Mo	1.2297 + 21
	Fe	5.5344 + 22
PuO_2-UO_2	^{235}U	1.9039 + 19
	^{238}U	1.3695 + 22
	^{239}Pu	4.6078 + 21
	^{240}Pu	1.2415 + 21
	^{241}Pu	1.3071 + 20
	^{242}Pu	2.2399 + 19
	O	4.3468 + 22

*Read as 2.3055×10^{22}.

110.200 MWd/kg. The normalized gamma source spectrum utilized is also given in Table 3.

A third transport calculation was performed (again utilizing only the gamma groups) to estimate the contribution due solely to prompt gammas from the fission reaction. This calculation assumed a uniform fixed source in each fuel pin, with the normalized distribution of source gammas per fission shown in the last column of Table 3.

As a result of the non-uniform flux distribution in the radial direction of the reactor core, the actual location of the fuel assembly

Table 3. Input Source and Response Functions for the Radiation Transport Calculations

Energy Group	Top Boundaries (MeV)	Energy Deposition Function for SS-316 $\frac{W/cm^3}{photons/cm^2\text{-}S}$	Decay Spectrum (photons/source photon)	Fission Gamma Spectrum (photons/source photon)
1	13.0	3.6498 - 13	1.7100 - 16	0.0
2	10.1970	2.6968 - 13	2.6007 - 08	1.1131 - 05
3	7.9983	1.9937 - 13	5.3812 - 07	1.2874 - 03
4	6.2737	1.5210 - 13	1.9810 - 04	4.5724 - 03
5	4.9210	1.1794 - 13	1.0780 - 03	1.1051 - 02
6	3.8599	9.2545 - 14	2.3419 - 03	1.9155 - 02
7	3.0277	7.4020 - 14	1.0250 - 02	3.1698 - 02
8	2.3748	6.0437 - 14	1.4787 - 02	3.9787 - 02
9	1.8628	4.9966 - 14	2.8168 - 02	5.1099 - 02
10	1.4611	4.1527 - 14	5.0087 - 02	8.0031 - 02
11	1.1461	3.4407 - 14	6.1957 - 02	8.6622 - 02
12	0.89896	2.8241 - 14	1.1385 - 01	1.0010 - 01
13	0.70513	2.3037 - 14	7.4116 - 02	1.1902 - 01
14	0.55309	1.8819 - 14	8.4076 - 02	1.0357 - 01
15	0.43383	1.5639 - 14	4.3326 - 02	8.6573 - 02
16	0.34029	1.3588 - 14	7.4641 - 02	6.9508 - 02
17	0.26692	1.2873 - 14	5.9827 - 02	5.3163 - 02
18	0.20937	1.3843 - 14	4.5466 - 02	4.7227 - 02
19	0.16422	1.7221 - 14	4.4408 - 02	3.2214 - 02
20	0.12881	2.4195 - 14	5.5077 - 02	2.2129 - 02
21	0.10104	3.6714 - 14	5.6432 - 02	1.4283 - 02
22	0.079252	5.8095 - 14	5.5477 - 02	1.0150 - 02
23	0.062164	9.3590 - 14	4.0994 - 02	7.1159 - 03
24	0.048760	1.5138 - 13	4.5487 - 02	4.4562 - 03
-	0.03			

containing the gamma thermometer in the core grid pattern may have a direct effect on the energy deposition rate within the GT. To assess this effect (i.e., the uncertainty in the location of the instrumented fuel assemblies), the preliminary investigation included two cases that utilized boundary conditions for the radiation transport calculations representing extreme conditions. The first calculation was performed using the two fixed sources (fission source and fission-product decay source) and fully reflected boundary conditions (i.e., infinite lattice of fuel assemblies) on all sides. The second set of calculations was performed for the same two fixed sources but utilizing a vacuum boundary condition (an isolated element) on the outermost radial boundary. The results of this analysis (given in Table 4) show that approximately 82% of the fission gammas and 84% of the fission-product gammas originate within the instrumented fuel element. These results indicate that the response of the GT will be relatively insensitive to the actual location of the instrumented fuel assembly within the reactor core since the primary contributions are from within the assembly itself. The remainder of this report, unless otherwise stated, will consider only the fully reflected case for clarity. The results reported for the fully reflected case are not modified significantly if the boundary conditions on the exterior of the fuel assembly are changed to consider less than fully reflective conditions.

Table 4. Fraction of Total Response Due to Gammas Originating Within the Fuel Assembly Containing the Gamma Thermometer

Source	Fraction of Signal
Fission	0.8235
Decay	0.8443

One overall objective of the forward transport analysis was to determine the spatial distribution of the energy deposition within the GT. The results of that analysis, however, indicated a flat spatial distribution within the GT, with the maximum spatial deviation from the

centerline value being approximately 1% for the fission-product decay case. All other cases indicate a spatial deviation from the centerline value of less than 0.5%.

Table 5 presents a source breakdown of the total energy deposited in the GT during normal operation of an LMFBR. The importance of the other (non-fission) neutron-induced reactions to the total heat deposition rate is exemplified by this result. The fractional breakdown of the total source by gamma production process (i.e., fission-product decay, fission, etc.) is also depicted in Table 5. These results indicate a total response breakdown of approximately 16.0% from fission-product decay, 25.4% from fission gammas, 49.3% from other neutron-induced reactions (e.g. capture, inelastic), and 9.3% from direct neutron heating. A further characterization of the total neutron-induced response (excluding fission-product decay) yields a percentage breakdown of 30.2% resulting from fission gammas, 58.7% from other neutron-induced gammas, and 11.1% from neutron heating.

Table 5. Breakdown (by Source) of the Total Volumetric Energy Deposition Rate within the Gamma Thermometer

Source of Particle	Volumetric Energy Deposition Rate (W/cm^3)	Fraction of Total Response
Fission-product decay γ	11.75	0.1603
Fission γ	18.61	0.2540
Neutron-induced γ (non-fission)	36.15	0.4932
Neutron heating	6.78	0.0925
Total	73.29	1.0000

As a secondary objective, the spatial distribution of the source gammas contributing to the effect of interest was also characterized. To this end, a set of adjoint gamma transport calculations was executed. The logical 9n-25γ group coupled adjoint case was not executed because the DOT-IV code does not yet include provision for such a generalized adjoint calculation (i.e., fixed source in a critical reactor). The

source for the adjoint cases was the response function (see Table 3) used in the forward transport analysis (i.e., the energy deposition function for stainless steel). The response functions for the adjoint transport analysis were the fission gamma source spectrum and fission-product decay gamma source spectrum, also presented in Table 3.

The radial characterization of the gamma source is presented in Table 6. Only the prompt fission gamma and fission-product decay gamma data were calculated. In Table 6 the fuel pin numbers correspond to those presented in Fig. 4, and partial fuel pin contributions were adjusted to represent a whole fuel pin even though the analysis modeled only half fuel pins along the symmetry boundaries. Comparison of the two reflective cases in Table 6 indicate that the fractional contribution by decay gammas is slightly higher in the rows immediately adjacent to the GT and lower in the fuel pin rows farther away than are contributions by prompt fission gammas. This result is seen more clearly in Table 7, which shows approximately 50% of the response attributable to fission-induced gammas originates in the first three rows of elements, whereas approximately 54% of the response attributable to fission-product decay gammas originates in the first three rows in the fully reflected case. Likewise, the results show a 57%-62% split for the void case. These results indicate that the GT is, as desired, strongly dependent on the localized power generation rate.

To further characterize the forward gamma source, and to investigate the contribution of the various materials, a sensitivity study was performed. Using the coupled 9n-25γ group eigenvalue fluxes and the adjoint 25γ group fluxes, the contributon flux ($\phi\phi^*$) by material region was calculated using the VIP[9] computer code. The sensitivity analysis was performed using SWANLAKE[10] to fold the contributon flux with a partial cross-section sensitivity library (i.e., the 9n-25γ group library, broken up by element). The results of the sensitivity analysis by mixture are presented in Table 8, with the results by element for the mixtures presented in Tables 9 and 10.

The characterization of the neutron-induced response by material (Table 8) yields 93.7% originating in the fuel-clad mixture, 1.4% originating

Table 6. Fractional Contribution by Fuel Pin to the Total Volumetric Energy Deposition Rate in the GT for Reflected and Void Boundary Conditions

Fuel Pin No.	Fission (reflected)	Decay (reflected)	Fission (void)	Decay (void)
1	0.03197	0.03698	0.03782	0.04311
2	0.01242	0.01302	0.01410	0.01474
3	0.00688	0.00686	0.00738	0.00744
4	0.00456	0.00436	0.00456	0.00447
5	0.00324	0.00298	0.00294	0.00281
6	0.00244	0.00216	0.00197	0.00182
7	0.00190	0.00163	0.00133	0.00119
8	0.00153	0.00128	0.00093	0.00081
9	0.01549	0.01666	0.01783	0.01905
10	0.00824	0.00833	0.00903	0.00919
11	0.00552	0.00530	0.00564	0.00553
12	0.00346	0.00317	0.00323	0.00305
13	0.00259	0.00229	0.00217	0.00199
14	0.00206	0.00178	0.00152	0.00137
15	0.00152	0.00129	0.00098	0.00086
16	0.00473	0.00456	0.00488	0.00480
17	0.00378	0.00350	0.00360	0.00344
18	0.00280	0.00250	0.00241	0.00223
19	0.00220	0.00191	0.00167	0.00150
20	0.00183	0.00155	0.00120	0.00106
21	0.00294	0.00265	0.00257	0.00241
22	0.00230	0.00200	0.00178	0.00162
23	0.00188	0.00160	0.00128	0.00135
24	0.00193	0.00164	0.00133	0.00118

Table 7. Fractional Contribution by Fuel Pin Row to the Total Volumetric Energy Deposition Rate

Row	Number of Fuel Pins	Fission (refl)	Decay (refl)	Fission (void)	Decay (void)
1	0				
2	6	0.1918	0.2219	0.2269	0.2587
3	12	0.1675	0.1781	0.1916	0.2027
4	18	0.1402	0.1411	0.1526	0.1549
5	24	0.1220	0.1171	0.1243	0.1220
6	30	0.1063	0.0979	0.0996	0.0947
7	36	0.0970	0.0863	0.0822	0.0760
8	42	0.0901	0.0781	0.0676	0.0610
9	48	0.0835	0.0708	0.0551	0.0512

Table 8. Fractional Contribution by Mixture to the Volumetric Energy Deposition Rate

Mixture	Material	Fractional Contribution
Fuel + Clad	(PuO_2UO_2) + (SS-316)	0.9365
Coolant	Na	0.0140
Fuel Assembly Casing	SS-316	0.0224
Gamma Thermometer	SS-316	0.0283

Table 9. Fractional Contribution by Material of the Total Volumetric Energy Deposition Rate Due to Fuel + Clad

Material	Fractional Contribution
^{235}U	0.0028
^{238}U	0.1544
^{239}Pu	0.6730
^{240}Pu	0.0500
^{241}Pu	0.0110
^{242}Pu	0.0003
Fe	0.0234
Cr	0.0090
Ni	0.0073
Si	0.0003
Mn	0.0017
Mo	0.0033

Table 10. Fractional Contribution by Material of the Total Volumetric Energy Deposition Rate Due to Fuel Assembly Casing and Gamma Thermometer

Material	Fractional Contribution (fuel assembly casing)	Fractional Contribution (gamma thermometer)
Fe	0.0111	0.0147
Cr	0.0046	0.0061
Ni	0.0038	0.0041
Si	0.0001	0.0001
Mn	0.0010	0.0013
Mo	0.0018	0.0021

in the sodium coolant, 2.2% originating in the fuel element cladding (SS-316), and 2.8% originating in the GT itself. Further characterization indicates that the major contributors in the fuel-clad mixture (Table 9) are ^{239}Pu-67%, ^{238}U-15%, and ^{240}Pu-5%, whereas in the fuel assembly cladding (Table 10) and within the GT itself (Table 10), Fe was the major contributor to the response.

The primary results of the transport analysis indicate that the majority (approximately 84%) of the energy deposition rate is due to neutron-induced reactions and 16% is due to fission-product decay. A second indication is that approximately 83% of the gamma source originates within the instrumented fuel assembly and therefore the GT response will be somewhat dependent on the instrumented assembly's location in the core. The final results indicate that approximately 1.4% of the neutron-induced gamma source originates in the sodium coolant, 93.6% in the fuel-clad mixture, 2.8% within the thermometer itself, and 2.2% from the fuel assembly cladding.

IV. THERMAL-HYDRAULIC ANALYSIS

4.0 Introduction

In addition to the characterization of the radiation field in the vicinity of the GT, its response to changes in the thermal-hydraulic environment is also of interest. This is particularly true concerning the proposed local power level monitor mode of operation. Although the one-dimensional calculations discussed in Chapter II established the theoretical feasibility of such a power level monitor, verification of the "robustness" of the signal to detailed geometric modeling as well as to the actual time-dependent fluid property changes must be established. To investigate the effects of coolant-related parameters on the GT signal, a prototypic calculational model of the GT (depicted in Fig. 5) was created. The transient heat conduction code HEATING-5[11] was used to calculate the spatial and time dependence of the GT signal. The coolant parameters utilized were typical of the thermal-hydraulic environment

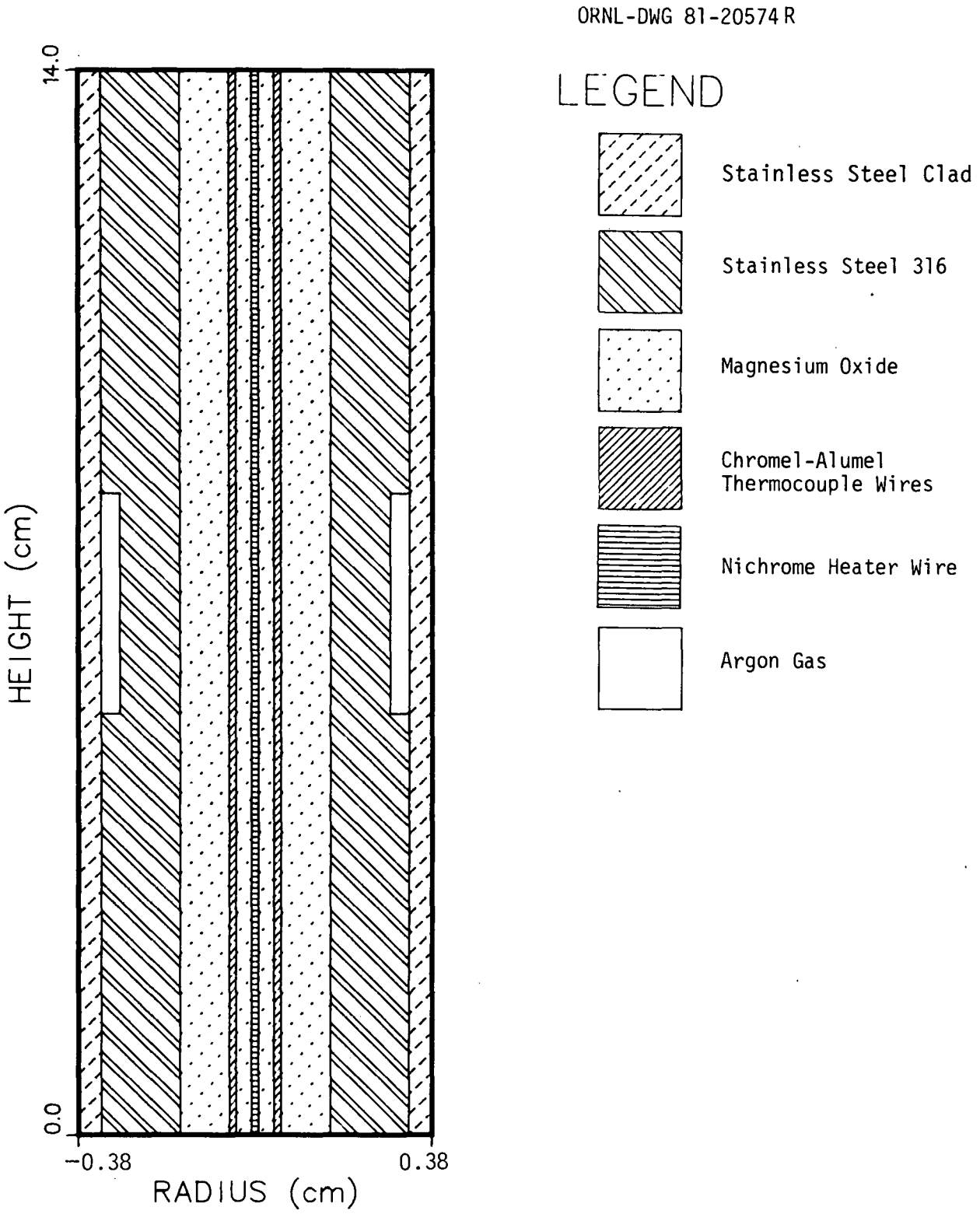

Fig. 5. Computational Model of the Gamma Thermometer Used for the Thermal Hydraulic Analysis.

within an LMFBR fuel assembly (see Table 1). Further, the analysis incorporated the volumetric heat source obtained via the radiation transport calculations. Temperature-dependent material properties were utilized for each material, with the data being extracted from the Nuclear Systems Materials Handbook.[12]

The analyses considered the behavior of the GT signal during normal reactor operating conditions as well as during and subsequent to various reactor transients. The transients analyzed were: (1) a reactor scram modeled as an instantaneous termination of the gamma source attributable to neutron-induced reactions, and (2) an instantaneous sodium coolant flow blockage modeled as an instantaneous change in the external heat transfer coefficient from approximately 81,500 $W/m^2°C$ (which represents normal reactor core conditions) to approximately 34,600 $W/m^2°C$ (which is assumed to represent stagnant sodium).

4.1 Sensitivity of Power Level Monitor to the Thermal-Hydraulic Conditions

In analyzing the applicability of the GT as a localized power level monitor, two characteristic parameters of the generic GT are of interest: the calibration of the device with respect to the local heat generation rate (LHGR), and the time constant of the instrument itself. The fundamental relationship between the LHGR and the temperature differential between the "hot" and "cold" thermocouple junctions is postulated as [see Eq. (4)]:

$$(T_{Hot} - T_{Cold}) = a \cdot \text{LHGR} + b \ , \qquad (5)$$

where a is the proportionality constant relating the local heat generation rate to the temperature differential and b is an adjustment factor, required since the ratio of fission-product LHGR to total LHGR is not identical to the ratio of fission-product GT signal to total GT signal. It should be noted that a will depend on the fuel assembly geometry as well as on the GT materials and geometry. Thus, the linear power inferred from the GT signal can be expressed as:

$$LHGR^* = \alpha \cdot (T_{Hot} - T_{Cold}) + \beta \quad . \qquad (6)$$

Based on the radiation transport analysis presented in the previous section, and on a series of static thermal-hydraulic calculations using the HEATING-5 computer code, the value of α was calculated to be 1.3574 W/cm · °C, and β was estimated as -49.1286 W/cm. This relationship is depicted in Fig. 6, which represents the relationship between the local heat generation rate and the GT response for a reactor core after 550 equivalent full-power days of operation. By employing the calibration curves (Fig. 6) in conjunction with the local power level monitor response curves (Fig. 7), a system capable of tracking changes in the local power level (due to control rod movement, burnup, etc.) is realized. It should be noted that the curves (Figs. 6 and 7) do not have a zero intercept (i.e., zero power does not imply zero ΔT). The principal reason behind this characteristic is the buildup and subsequent decay of fission products, which accounts for approximately 3% of the total thermal power generated. The gammas contributed by reactions representing 3% of the total thermal power, however, contribute 16% of the GT signal (see discussion in Chapter III). This result indicates that b in Eq. (5) and β in Eq. (6) are both functions of the reactor burnup (i.e., the amount of fission products present). However, since the fission-product concentrations and consequently the fission-product gamma source reach an asymptotic value after only a few days of full-power operation,[13] β will essentially be a constant value except for a short time following initial reactor start-up (or restart). It should be noted that for a cold clean core (i.e., no fission products), the initial value of β would be zero and the resulting calibration curve would probably parallel the curve in Fig. 6. Verification of this characteristic would require knowledge of the behavior of α as a function of burnup, which is beyond the scope of this investigation.

The second characteristic of the GT that affects its applicability as a local power level monitor is the time constant of the instrument itself. In Eq. (6), a relationship between the GT signal ($T_{Hot} - T_{Cold}$) and the inferred LHGR* is given. Utilizing the values for α and β, and the differential temperature reading from a transient HEATING-5 calculation

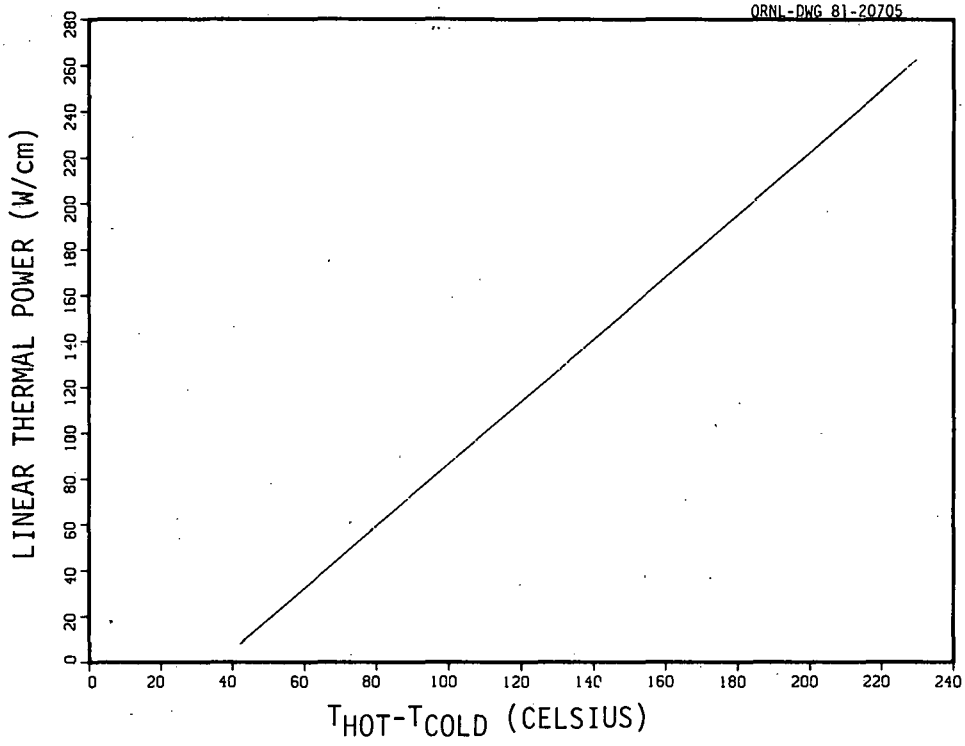

Fig. 6. Calibration Curve for the Power Level Monitor (110.2 MWd/kg Burnup).

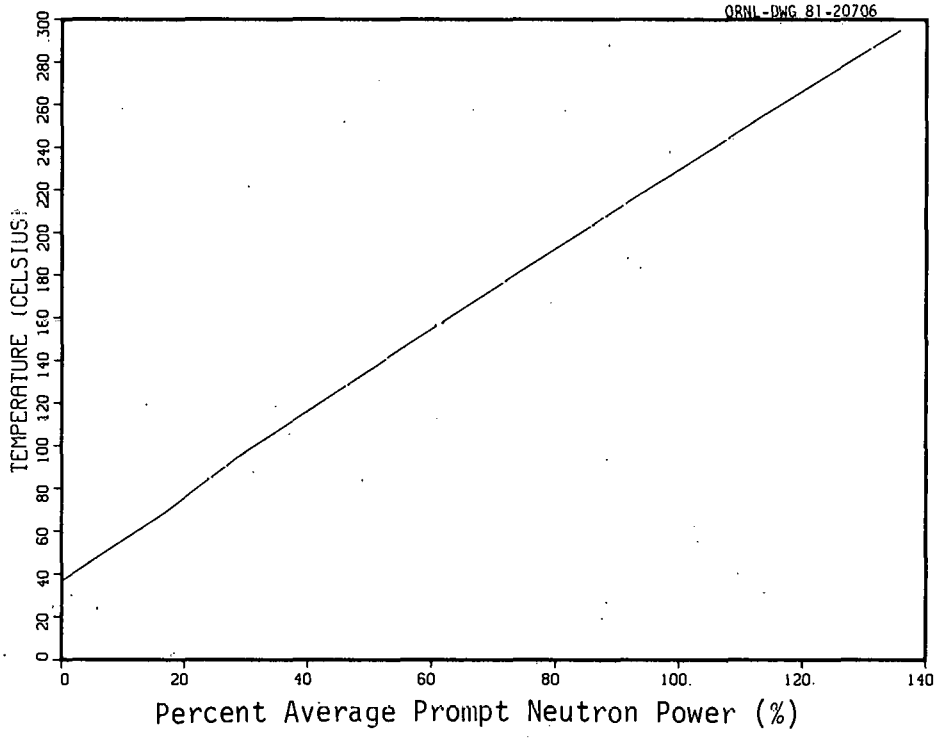

Fig. 7. Power Level Monitor Response to Changes in the Average Prompt Neutron Power.

modeling an instantaneous reactor scram, a comparison of the actual LHGR and inferred LHGR* was made and is shown in Fig. 8. The results presented in Fig. 8 indicate that the GT attained the new power level reading approximately 60 s after the transient commenced. The thermocouple response time constant was estimated to be 0.1056 °C/s, assuming an exponential relationship between ΔT and time.

The results of the one-dimensional calculations indicated that the local power level indicator reading of the GT ($T_{Hot} - T_{Cold}$) would be a strong function of the reactor power but a relatively weak function of the thermal-hydraulic environment of the GT (principally, the external heat transfer coefficient). The preliminary indication is confirmed by these more detailed calculations. Figure 9 depicts the time-dependent local power level indication (i.e., GT signal) as a result of an instantaneous reactor scram. The results indicate a factor of 5.5 change in the GT signal and therefore confirm the strong dependence of the GT signal on the local power level, as indicated by the one-dimensional analysis. The time dependence of the local power level indication for an instantaneous sodium flow blockage (depicted in Fig. 10) is seen to remain virtually constant, which further exemplifies the insensitivity of the local power level indicator to the thermal-hydraulic environment. As a final confirmation of the one-dimensional analytical results, a combination instantaneous reactor scram and sodium flow blockage was modeled in HEATING-5. The results for the local power level monitor, however, traced the results for the instantaneous reactor scram (Fig. 9) exactly and therefore is not indicated separately. This result indicates that the measured signal change is due primarily to the power level change and therefore is insensitive to the thermal-hydraulic environment within the fuel assembly containing the GT.

The results presented in this section appear to suggest that the time-dependent local power level indicator was shown to be a strong function of the reactor power for the case of the reactor scram (Fig. 9), yet insensitive to the thermal-hydraulic environment as seen in the time response to a sodium flow blockage (Fig. 10). Therefore the use of the GT as a local power level monitor is feasible with an adequately strong signal for interpretation.

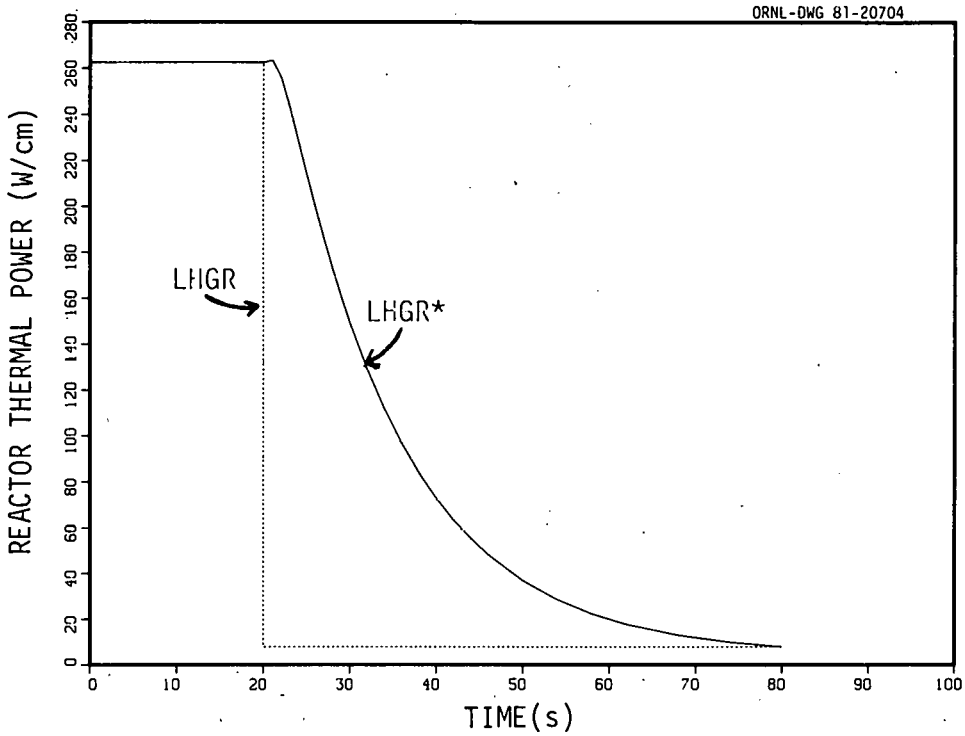

Fig. 8. Comparison of the Actual (LHGR) Versus Inferred (LHGR*) Reactor Power Subsequent to an Instantaneous Reactor Scram.

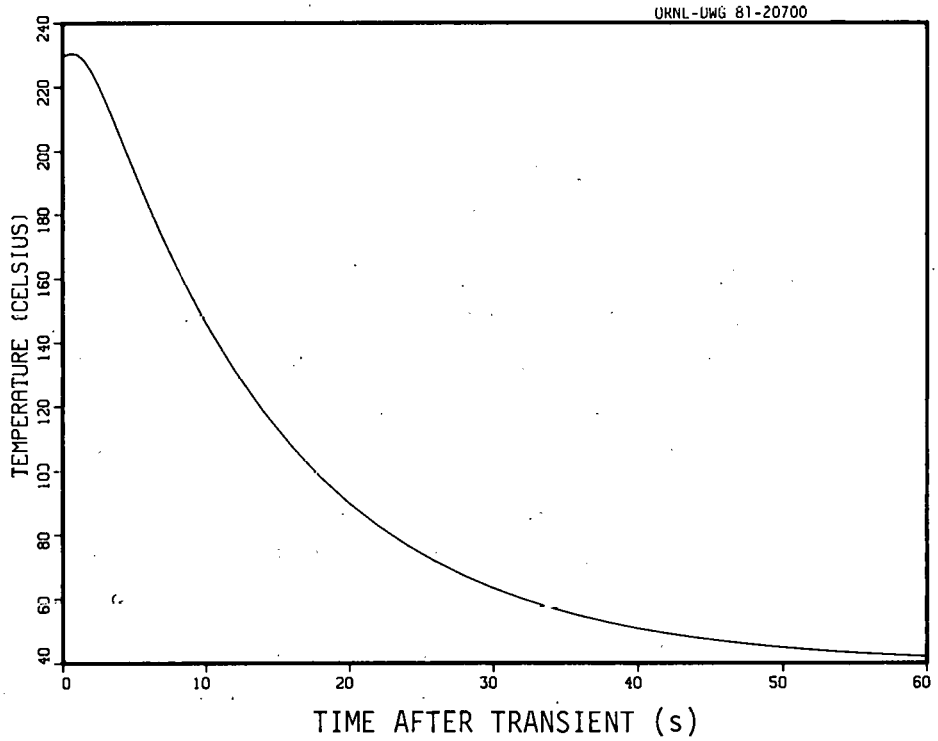

Fig. 9. Power Level Monitor Response Subsequent to an Instantaneous Reactor Scram.

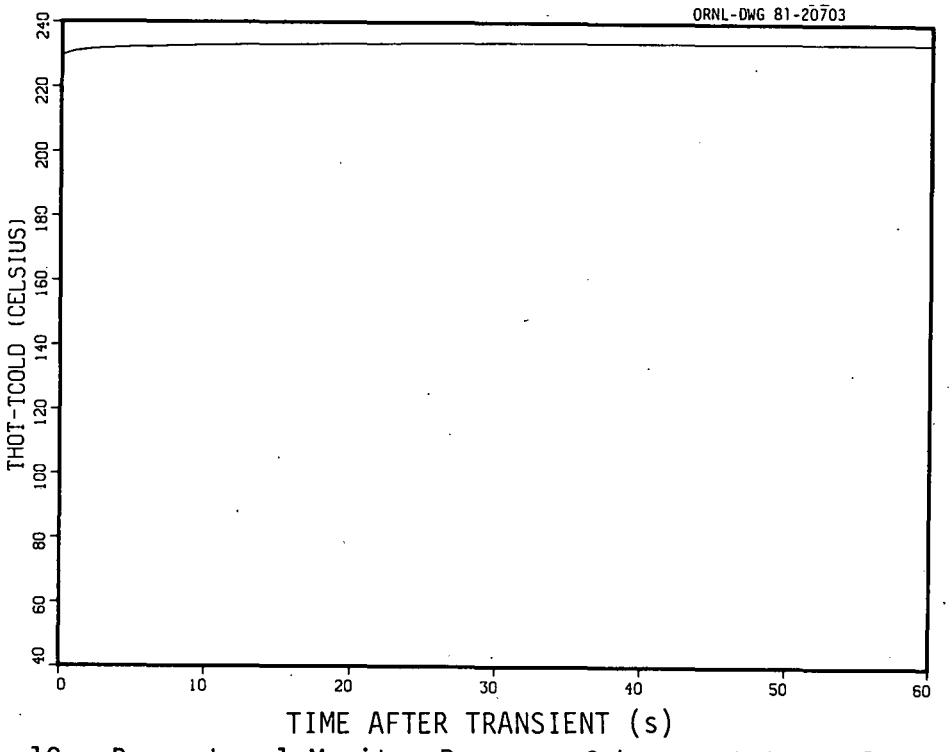

Fig. 10. Power Level Monitor Response Subsequent to an Instantaneous Sodium Coolant Flow Blockage.

4.2 Use of the Gamma Thermometer as a Possible Sodium Flow Blockage Monitor (SFBM)

The investigation of the gamma thermometer as a possible sodium flow blockage monitor (SFBM) is based primarily on the positive results indicated in the previous PWR studies[3,4] which analyzed the operation of the GT as an adequate core cooling monitor (ACCM). Operation of the GT in this mode is principally due to the fact that the heat transfer coefficient on the exterior surface of the device depends on the state of the coolant medium within the fuel assembly. The radial heat transfer characteristics at the hot and cold thermocouple locations are radically different under normal reactor operations (i.e., with the active region of the GT immersed in coolant). The radial heat flow at the hot thermocouple is sharply reduced by the gas gap (which functions as an insulator). Therefore, the heat flow in this region is principally in the axial direction. By way of contrast, the radial heat flow at the cold thermocouple is relatively unrestricted during normal operation. This differential heat transfer

results in a relatively higher temperature at the hot thermocouple. Therefore, a decrease in the heat removal capacity of the coolant medium (i.e., a decrease in the exterior heat transfer coefficient via flow blockage) will be reflected as a reduction of the temperature differential between the two thermocouple locations as well as higher absolute temperatures for both locations if the volumetric source remains constant. It is hypothesized that the temperature differential (as measured by the thermocouple) can be used to indicate the presence or absence of the coolant flow in that particular fuel assembly.

4.2.1 Design Modifications to Include Sodium Flow Blockage Detection

The use of the GT as a possible sodium flow blockage monitor is dependent on the ability of the device to indicate changes in the sodium flow rate (via the exterior heat transfer coefficient) without compromising its use as a local power level monitor. Consequently, the signal utilized for the flow blockage monitor must be a weak function of the reactor power and a strong function of the heat transfer and thermal-hydraulic characteristics of the fuel assembly -- exactly the opposite of the signal requirements for the power level mode of operation.

In light of the desire to produce a flow blockage monitor response with the above characteristics, a simple expedient is to divide Eq. (2) by Eq. (3) (see Chapter II), thereby eliminating the dependence on q, giving:

$$\frac{(T_{Hot} - T_{Coolant})}{(T_{Cold} - T_{Coolant})} = \frac{\frac{L_1^2}{2}(1 - e^{-2mL_2}) + \frac{L_1 R_1^2}{mR_2^2}(1 + e^{-2mL_2}) + \frac{1}{m^2}(1 - e^{-2mL_2})}{\frac{2L_1 R_1^2}{mR_2^2} e^{-mL_2} + \frac{1}{m^2}(1 - e^{-2mL_2})} \cdot (7)$$

Figure 11 illustrates the relationship shown in Eq. (7) and verifies the strong dependence of the ratio of the thermocouple signals on the exterior heat transfer coefficient. Although Eq. (7) possesses the desired characteristics, the ratio specified requires that additional information be incorporated into the response. In particular, it requires that two absolute

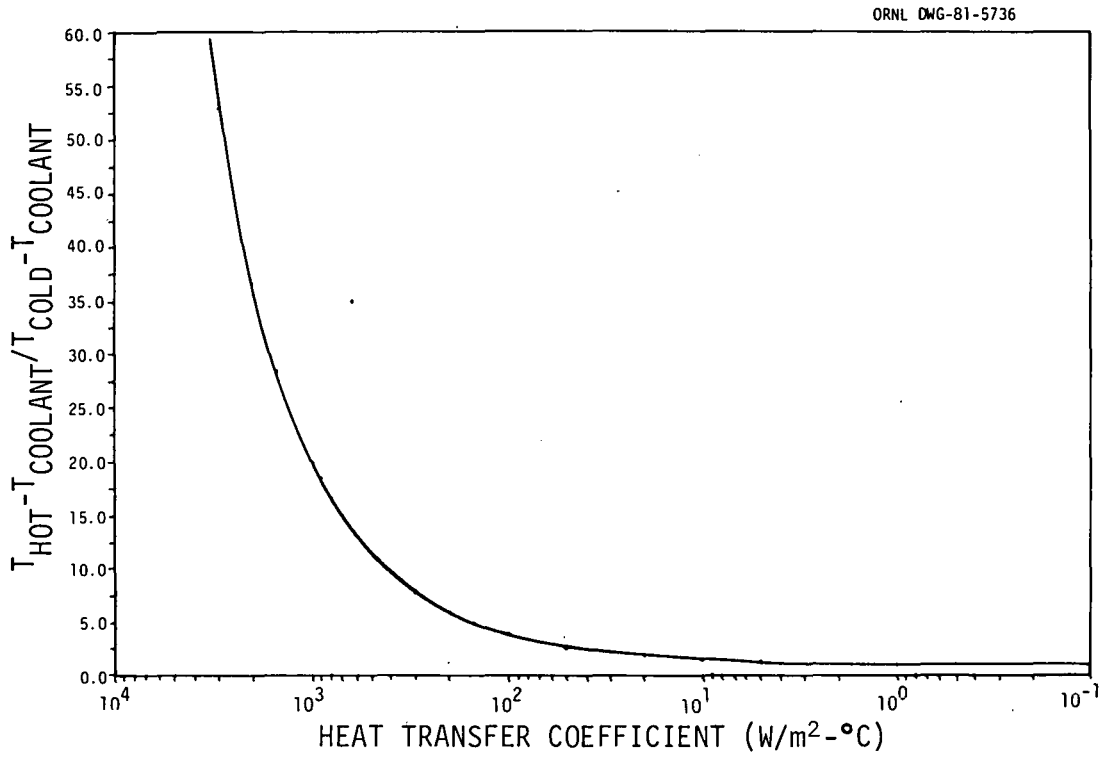

Fig. 11. Theoretical Fluid Level Characteristics of the Standard Gamma Thermometer Using the Coolant Temperature as the Reference Temperature.

temperature measurements (or one absolute and one differential measurement) as well as an external measurement of the coolant temperature be available.

To remedy this situation of relying on information from external measurements, a slightly modified version of the GT can be utilized. The modification consists of incorporating a third thermocouple junction between the hot and cold junctions of the standard design (see Fig. 1). This will result in a device (Fig. 12) which contains a "dual-differential" thermocouple (Fig. 13) capable of measuring both the local power level response and a potential flow blockage response.

Theoretically, an alternate response that is insensitive to the power level can be constructed by utilizing the additional temperature measurement at the point between the hot and cold junctions (given as T_{mid} in Figs. 12 and 13). Reflecting a relationship similar to that given in Eqs. (1) and (2), the temperature at this point is given by:

$$(T_{Mid} - T_{Coolant}) = \frac{\frac{qL_1R_1^2}{kmR_2^2}\ (1 + e^{-2mL_2})}{(1 - e^{-2mL_2})} + \frac{q}{m^2k} \qquad (8)$$

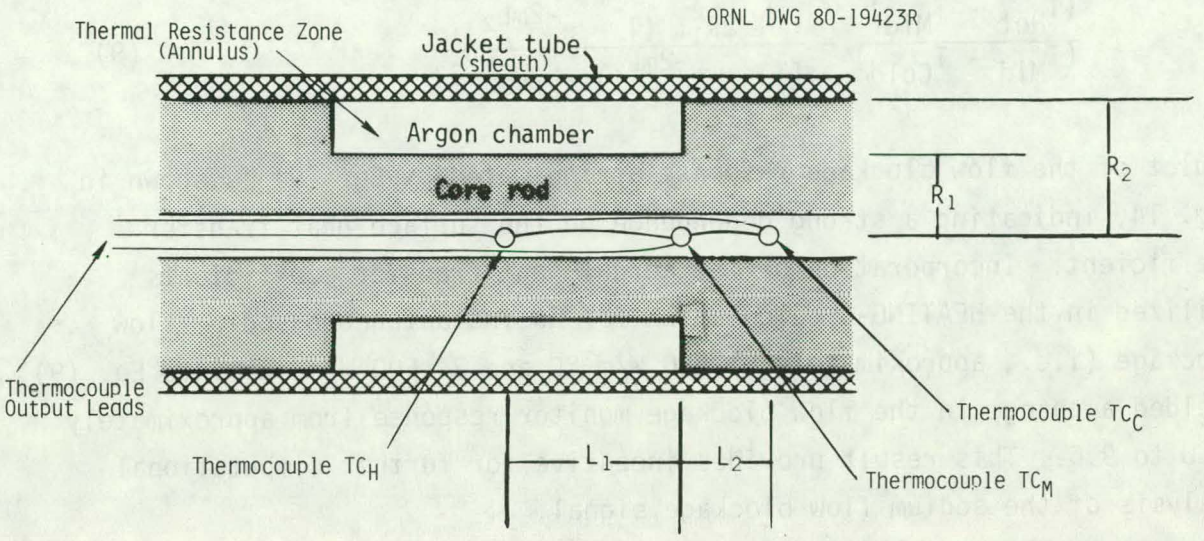

Fig. 12. Schematic of the Modified Gamma Thermometer.

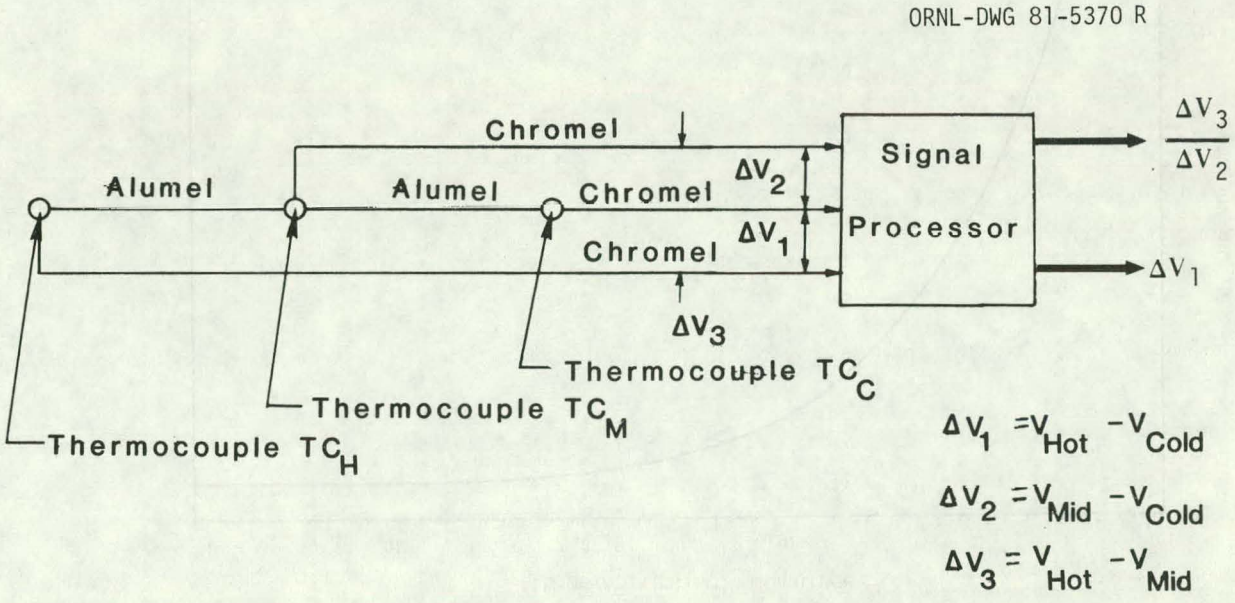

Fig. 13. Schematic of the Modified Gamma Thermometer Thermocouple Design.

so that the proposed flow blockage response is given by:

$$\frac{(T_{Hot} - T_{Mid})}{(T_{Mid} - T_{Cold})} = \frac{\frac{mL_1R_2^2}{2R_1^2}(1 - e^{-2mL_2})}{[(1 + e^{-2mL_2}) - 2e^{-mL_2}]} \quad . \tag{9}$$

A plot of the flow blockage response as indicated by Eq. (9) is shown in Fig. 14, indicating a strong dependence on the surface heat transfer coefficient. Incorporation of the actual heat transfer coefficients utilized in the HEATING-5 calculation for an instantaneous sodium flow blockage (i.e., approximately 81,500 $W/m^2°C$ and 34,600 $W/m^2°C$) into Eq. (9) yielded a change in the flow blockage monitor response from approximately 14.0 to 9.6. This result provides incentive for further computational analysis of the sodium flow blockage signal.

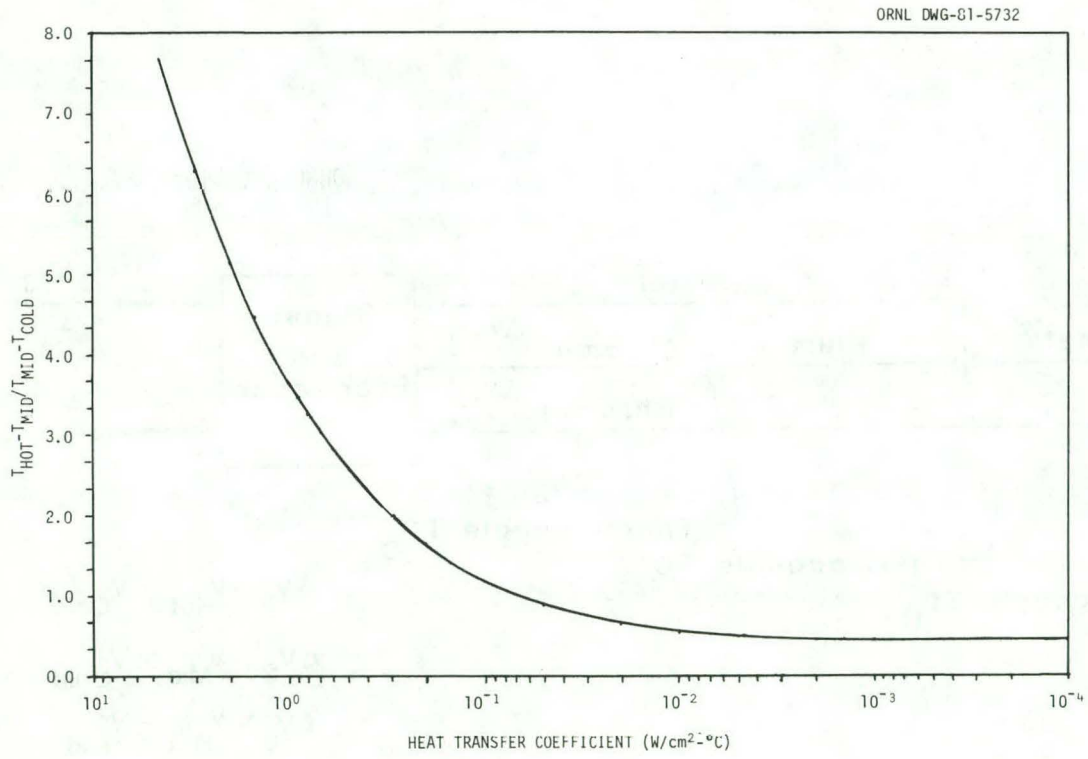

Fig. 14. Theoretical Fluid Level Characteristics of the Modified Gamma Thermometer Using an Internal Temperature as the Reference Temperature.

Analogous to the response of Eq. (7), this response is nominally independent of the power level. Moreover, it requires no information not available from thermocouple measurements within the GT (i.e., the instrument is self-contained). A relatively straightforward manner of obtaining the requisite information is to measure $T_{Hot} - T_{Mid}$ (ΔV_3 in Fig. 13) with one differential TC and $T_{Mid} - T_{Cold}$ (ΔV_2 in Fig. 13) with another differential TC in series with the first TC, as shown in Fig. 13. The ratio of the two signals would yield the sodium flow blockage signal, and the sum of the two signals would yield the local power level signal. Alternatively, a pair of differential thermocouples (4 leads versus 3) can be constructed and used.

Analogous to the local power level monitor analysis, the local thermal-hydraulic conditions should be measurable using Eq. (9) as a response. The above theoretical analysis, however, merely illustrates the potential feasibility of using the GT as a sodium flow blockage monitor. Further numerical analysis is required to evaluate the assumptions utilized to characterize the response.

4.2.2 Results as a Flow Blockage Monitor

The results of the one-dimensional calculation presented above indicated that the sodium flow blockage monitor reading of the GT $(T_{Hot} - T_{Mid})/(T_{Mid} - T_{Cold})$ would be a strong function of the thermal-hydraulic environment but virtually independent of the reactor power. To verify this result and determine the robustness of the sodium flow blockage signal, the modified GT was analyzed for behavior during normal reactor operating conditions and during and subsequent to the reactor transients used in the local power level signal characterizations.

As indicated in Fig. 15, however, the anticipated response of the proposed indicator to the transient - an instantaneous decrease in the sodium velocity - cannot be considered to be robust. Although the results do show a slight decrease in the signal, this decrease is well within the error band of the differential thermocouples. Hence the interpretability of the signal is open to serious question. The primary reasons for this result are the high initial thermal conductivity of liquid sodium, coupled with the relatively small change (approximately 42%) in the exterior heat

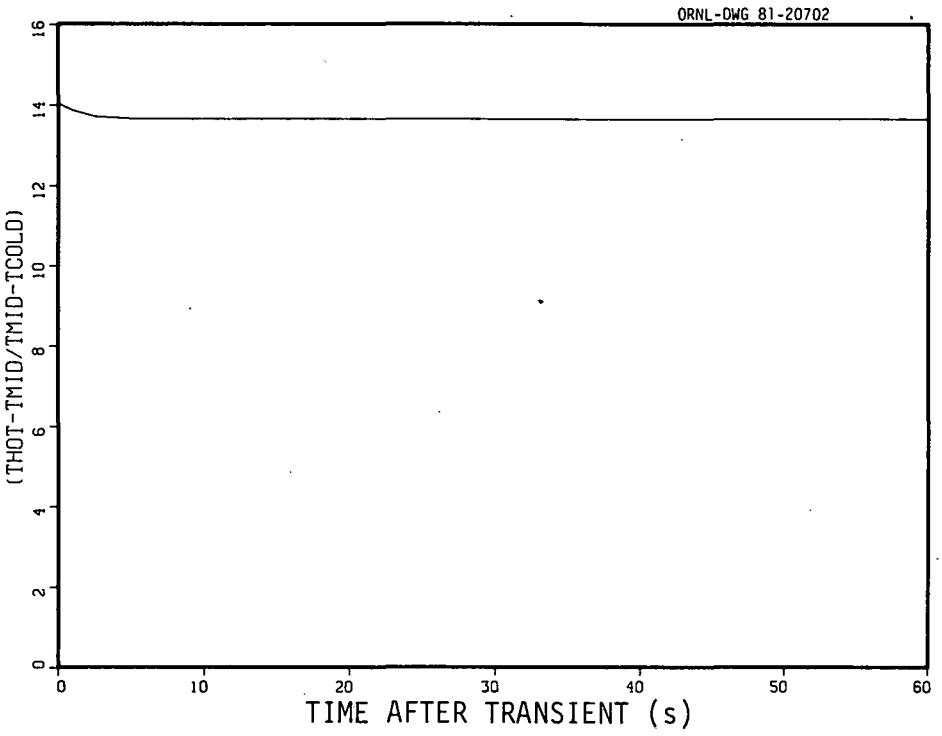

Fig. 15. Sodium Flow Blockage Monitor Response to an Instantaneous Sodium Flow Blockage.

transfer coefficient caused by the change from flowing sodium to stagnant sodium. Additionally, the calculation for the more realistic model used in the HEATING-5 calculation also results in a decrease in the potential signal. As shown in Fig. 16 (a plot of the centerline temperature distributions calculated via both methods), the effects of the simplifying assumptions used in the theoretical analysis are evident. Thus the use of the more realistic assumptions (i.e., two-dimensional heat transfer, temperature dependent properties, multimode heat transfer coefficients, etc.) in the HEATING-5 calculation resulted in a smoother, less sensitive temperature distribution and thereby decreased the change in the flow blockage signal response from approximately 4.4 (calculated via Eq. 9) to less than 1.0 (calculated via HEATING-5). The insensitivity of the sodium flow blockage indicator to the reactor scram, however, was upheld (see Fig. 17). The apparent noise in the signal is due to roundoff errors in the calculation and is within the error band of the differential thermocouples.

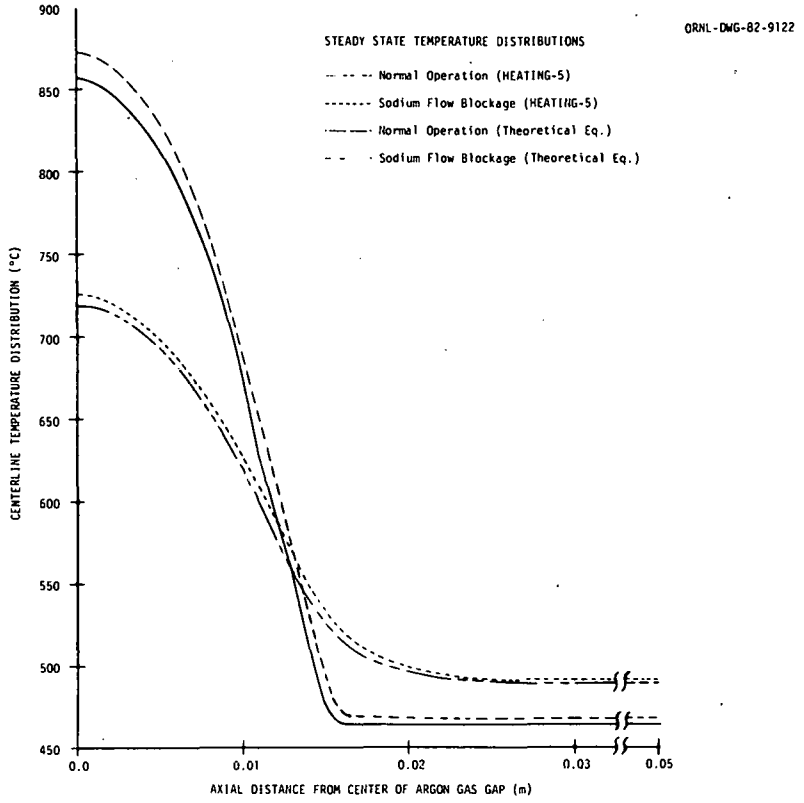

Fig. 16. Comparison of the Steady State Centerline Temperature Distributions Before and After a Sodium Flow Blockage.

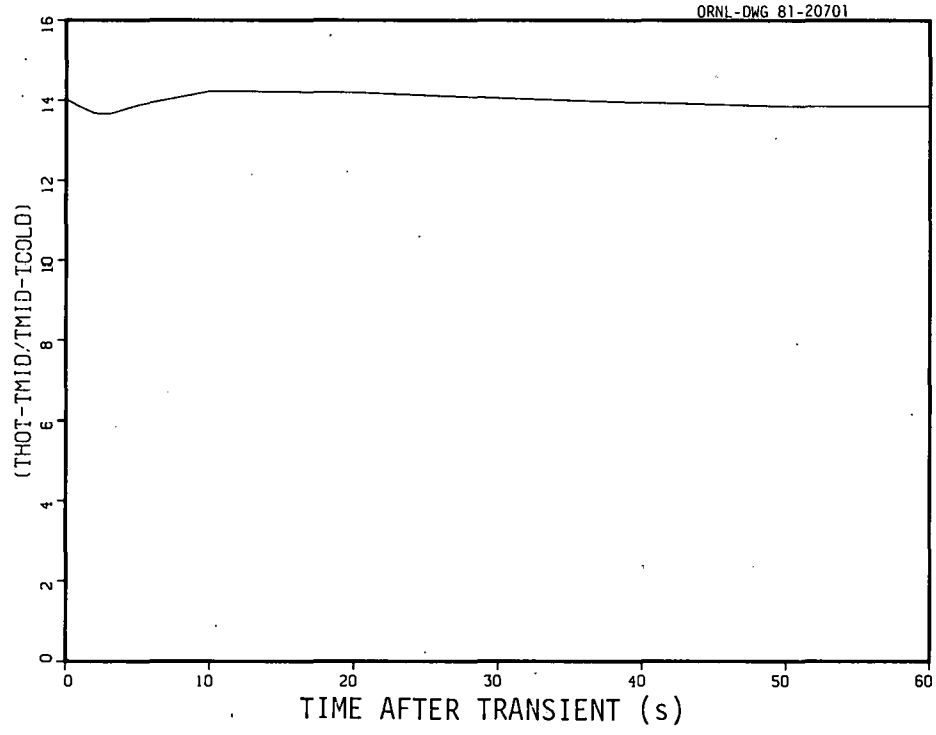

Fig. 17. Sodium Flow Blockage Monitor Response to an Instantaneous Sodium Flow Blockage.

As in the case of the local power level indication, a combination instantaneous reactor scram and sodium flow blockage calculation was executed to confirm the one-dimensional results. Analogous to the local power level indication results, these results indicated no discernible difference when compared to the results of the sodium flow blockage indication for a sodium flow blockage alone (i.e., the same slight drop in the signal; see Fig. 15). Hence, the potential for utilizing the gamma thermometer as a sodium flow blockage monitor (analogous to the PWR application) appears not to be feasible with the design studied.

V. CONCLUSIONS AND RECOMMENDATIONS

The initial contention that the gamma thermometer can be used as a local power level measurement device has been upheld by the more detailed calculations described in this report; however, utilization as a dual-purpose (i.e., both power level and sodium flow blockage) measurement device (analogous to the PWR case) was judged to be infeasible. The signal utilized to indicate the local power level is proportional to the LHGR and is insensitive to the thermal-hydraulic environment. Thus, it should be possible to infer the reactor power level regardless of changes in either the reactor power or thermal-hydraulic environment. The sodium flow blockage indicator response to changes in the thermal-hydraulic environment (via the exterior heat transfer coefficient) was shown to be negligible.

The detailed characterization of the radiation field has determined, for the specific fuel assembly and GT model considered, the geometrical location of the various gamma sources relative to their importance to the GT signal, and has also characterized the materials that contribute to the response. Specifically, the particles responsible for the GT signal are produced primarily within the instrumented assembly itself (>83%). Moreover, approximately 52% of the signal is produced by particles originating within the first three rows of fuel pins (50% of the neutron-induced gammas and 54% of the fission-product decay gammas). Hence the GT signal is representative of the <u>local</u> heat generation rate (LHGR).

Of those gammas which contribute to the GT signal, 16% are traceable to the decay of fission products within the fuel pins (at 110,200 MWD/T burnup). Of the remaining 84% of the signal, 25% results from prompt fission gammas, 50% results from other neutron-induced reactions such as (n,γ) and $(n,n'\gamma)$, and 9% results from direct neutron heating. The total GT signal was also characterized by the material region in which the gammas were produced: 94% originated in the fuel pins, 1% in the coolant, 2% in the fuel assembly cladding, and 3% in the body of the GT itself.

Based on the results of the transport analyses, the GT power level signal calibration will depend on burnup. Since the gammas from fission products account for only 3% of the thermal power (with the reactor at full power) but 16% of the GT signal at a burnup of 110,200 MWD/T, the calibration curve for the device will result in a non-zero intercept in general. However, since the fission-product gamma source asymptotes rapidly ($\sim$a few full-power days), such an effect represents only an initial transient in the calibration curves for the start-up of the reactor (and possibly a transient on restart).

The thermal-hydraulic analyses described in this report have shown, in a preliminary sense, that although the GT signal information can be utilized to measure the LHGR, as presently configured it will not detect a sodium flow blockage. The results did, however, indicate that the local power level signal is relatively insensitive to the thermal-hydraulic environment and is readily interpretable. A reactor scram (decrease from 100% to 3% in thermal power) resulted in a reduction of the local power level signal by a factor of 5.5. Conversely, the proposed sodium flow blockage indication was judged to be non-interpretable. The simulated sodium flow blockage (at power) resulted in the flow blockage indication changing by only a slight amount (14.02 to 13.68).

Although the results obtained in this study provide both encouragement and incentive to pursue the GT as a viable nuclear instrument for local power level measurement, this study must be regarded as only a first step toward complete characterization of the device. In particular, the adequacy of the many approximations and assumptions necessary to perform this study must be validated. More specifically, the areas requiring further study or more detailed analysis are:

1. The effect of the two-dimensional discrete ordinates approximation. A three-dimensional Monte Carlo analysis is necessary to verify the overall LHGR-to-energy-deposition-rate relationship obtained in this study, and also to model the geometry more adequately using combinatorial geometry.
2. The effect of placing the GT in a blanket assembly (internal, upper, or lower) or possibly a control assembly.
3. The initial time dependence of the GT signal as a function of burnup. Since the isotopes of the fuel change nonlinearly with time, it is reasonable that the GT calibration will also vary nonlinearly as a function of fuel isotopes.
4. The durability of the GT to the harsh environment (temperature, radiation, etc.) with respect to the material characteristics of the GT body and thermocouples.
5. The influence of perturbations of the neutron field on the response of the GT. Not considered in this study were possible changes in the neutron field (via control rod movement, etc.) which will affect both the magnitude and the location of the gamma sources contributing to the response.
6. Continuation of the sensitivity analysis to include type of reaction (i.e., captive, inelastic, etc.).
7. Determination of how (and where) the GT can be installed in an LMFBR without requiring major reactor design changes.
8. The feasibility of monitoring the sodium flow rate utilizing two (or more) gamma thermometers at different axial locations within an instrumented fuel assembly. Clearly, the relatively small change in the exterior heat transfer coefficient at a single GT active regime has been shown to be inadequate for signal interpretation. However, by employing two GTs incorporating both an absolute TC and differential TC at each annular location (one in the lower section of the active core and the other in the upper section of the active core), the mass flow rate — and hence a measure of the sodium velocity — could possibly be inferred. This approach is based on the relationship

$$\int_{z_0}^{z_1} P(z)dz = \dot{m}C_p[T(z_1) - T(z_0)] \quad , \tag{10}$$

where $\dot{m}$ = mass flow rate of sodium,

C_p = sodium heat capacity, and

$T(z_i)$ = temperatures at the two GT locations.

Thus, if the axial power distribution $P(z)$ is known (perhaps via the local power level indication capability of the GT), the velocity of the sodium can be determined if certain simplifying assumptions can be made relative to the specific heat and density of the sodium.

THIS PAGE

WAS INTENTIONALLY

LEFT BLANK

REFERENCES

1. J. S. Stutheit, "Fast Response Gamma Thermometers," *Nucl. Instrum. Methods, 63,* 300-306 (1968).

2. R. H. Leyse and R. D. Smith, "Gamma Thermometer Developments for Light Water Reactors," *IEEE Transactions on Nuclear Science, NS-26,* 934-942 (1979).

3. T. J. Burns and J. O. Johnson, "Theoretical Characterization of a Dual Purpose Gamma Thermometer," ORNL/TM-7567 (January 1981).

4. J. O. Johnson and T. J. Burns, "Thermal Hydraulic Analysis of the Dual-Function Gamma Thermometer," ORNL/TM-8089 (December 1981).

5. L. R. Williams, Engineering Physics Division, ORNL, private communication (June 1981).

6. N. M. Greene, W. E. Ford III et al., "AMPX: A Modular Code System for Generating Coupled Multigroup Neutron-Gamma Libraries from ENDF/B," ORNL/TM-3706 (March 1976).

7. W. A. Rhoades, D. B. Simpson, R. L. Childs, and W. W. Engle, "The DOT-IV Two-Dimensional, Discrete-Ordinates Transport Code with Space-Dependent Mesh and Quadrature," ORNL/TM-6529 (January 1979).

8. M. J. Bell, "ORIGEN - The ORNL Isotope Generation and Depletion Code," ORNL/TM-4629 (1973).

9. E. T. Tomlinson, R. L. Childs, and R. A. Lillie, "DOS Perturbation Modules DGRAD/VIP/TPERT," ORNL/CSD/TM-116 (May 1980).

10. D. E. Bartine, F. R. Mynatt, and E. M. Oblow, "SWANLAKE, A computer Code Utilizing ANISN Radiation Transport Calculations for Cross Section Sensitivity Analysis," ORNL/TM-3809 (May 1973).

11. W. D. Turner, D. C. Elrod, and I. I. Simon-Tov, "HEATING-5 — An IBM 360 Heat Conduction Program," ORNL/CSD/TM-15 (1977).

12. *Nuclear Systems Materials Handbook,* Vo. 1, TID-26666, Hanford Engineering Development Laboratory, Richland, Washington.

13. M. M. El-Wakil, *Nuclear Heat Transport,* International Textbook Company (1971).

THIS PAGE

WAS INTENTIONALLY

LEFT BLANK

ORNL/TM-8233
Distribution Category UC-79d
Breeder Reactor Physics - Base

INTERNAL DISTRIBUTION

1-2. L. S. Abbott
3. D. E. Bartine
4-8. T. J. Burns
9. R. M. Carroll
10. T. E. Cole
11. G. F. Flanagan
12. Uri Gat
13. W. O. Harms
14. D. T. Ingersoll
15-19. J. O. Johnson
20-24. F. C. Maienschein
25. D. L. Moses
26. F. R. Mynatt
27. D. L. Selby
28. R. L. Shepard
29. C. O. Slater
30. D. B. Trauger
31. J. L. Wantland
32. A. Zucker
33. P. W. Dickson, Jr. (Consultant)
34. H. J. C. Kouts (Consultant)
35. W. B. Lowenstein (Consultant)
36. R. Wilson (Consultant)
37-38. Central Research Library
39. Y-12 Document Ref. Section
40-41. Laboratory Records Dept.
42. Laboratory Records ORNL, RC
43. ORNL Patent Office

EXTERNAL DISTRIBUTION

44. Office of the Assistant Manager for Energy Research and Development, DOE-ORO, Oak Ridge, TN 37830

45. H. B. Adams, Project Manager, Energy Demonstrations and Tech., Tennessee Valley Authority, 1300 Commerce Union Bank Bldg., Chattanooga, TN 37405

46. Henry Piper, Safety and Licensing Coordinator, Project Management Corp., Engineering Division, P.O. Box U, Oak Ridge, TN 37830

47. Dennis Bell, Technology for Energy Corporation, 10770 Dutchtown Road, Knoxville, TN 37922

University of Tennessee, Department of Nuclear Engineering, Knoxville, TN 37916
48. Dr. H. L. Dodds
49. Dr. T. W. Kerlin
50. Dr. P. F. Pasqua

CRBR Project Office, Oak Ridge, TN 37830
51. R. S. Booth
52. C. H. Fox, Jr.
53. N. N. Kaushal
54. W. L. Kelly
55. Chuck Wilson

56-191. Given Distribution as shown in TID-4500, Distribution Category UC-79d - Breeder Reactor Physics - Base

DO NOT MICROFILM